# Seasonal cycle and long-term trend of solar energy fluxes through Arctic sea ice

Stefanie Arndt [1]*, Marcel Nicolaus [1]

[1] Alfred-Wegener-Institut Helmholtz-Zentrum für Polar- und Meeresforschung, Bremerhaven, Bussestraße 24, 27570 Bremerhaven, Germany

* Correspondence to:
Stefanie Arndt
Alfred-Wegener-Institut Helmholtz-Zentrum für Polar- und Meeresforschung
Bussestraße 24
27570 Bremerhaven
Germany

E-Mail: stefanie.arndt@awi.de
Phone: +49 471 4831 2140
Fax: +49 471 4831 1797

**Abstract**

Arctic sea ice has not only decreased considerably during the last decades, but also changed its physical properties towards a thinner and more seasonal cover. These changes strongly impact the energy budget and might affect the ice-associated ecosystem of the Arctic. In this study we quantify shortwave energy fluxes through sea ice sufficiently well over large regions and during different seasons. Here, we present a new parameterization of light transmittance through sea ice for all seasons as a function of variable sea ice properties. The maximum monthly mean solar heat flux of $30\times10^{5}$ $Jm^{-2}$ occurs in June, accounting for an equivalent ice melt of approximately 30 cm per month. Furthermore, our results suggest that 96% of the total annual solar heat input occurs from May to August, during four months only. Applying the new parameterization on remote sensing and reanalysis data from 1979 to 2011, we find an increase in light transmission of 1.5%/year for all regions. Over 33 years, this means an increase in potential sea ice bottom melt of 63%. Sensitivity studies reveal that the results strongly depend on the timing of melt onset and the correct classification of ice types. Hence, these parameters are of great importance for quantifying under-ice radiation fluxes and the uncertainty of this parameterization. Assuming a two weeks earlier melt onset, the annual budget increases by 20%. Continuing the observed transition from Arctic multi- to first year sea ice could increase light transmittance by another 18 %.

## 1. Introduction

The evolution of Arctic sea ice towards a thinner, younger and more seasonal sea ice cover during the last few decades (e.g. Comiso, 2012;Haas et al., 2008;Maslanik et al., 2011;Maslanik et al., 2007) has a strong impact on the partitioning of solar energy between the atmosphere, the sea ice, and the ocean (e.g. 2011a;Perovich et al., 2007b;Wang et al., 2014). A general decrease of surface albedo (Perovich et al., 2011a), an earlier melt onset, and a longer melt season (Markus et al., 2009, updated) cause an increase in sea ice and snow melt (Perovich and Richter-Menge, 2009) and lead to higher absorption and transmission of solar irradiance (Nicolaus et al., 2012;Stroeve et al., 2014). Beyond the physical consequences of the observed changes, strong impacts on biological and geochemical processes are expected, like changes in habitat conditions for ice-associated organisms or changes in primary productivity (Arrigo et al., 2012;Deal et al., 2011;Popova et al., 2012).

Various studies showed the immediate link between sea ice energy and mass balance, as well as the impact of energy fluxes on physical properties of sea ice (Grenfell et al., 2006;Light et al., 2008;Perovich and Richter-Menge, 2009). Those heat fluxes are composed of short- and long-wave, conductive, as well as turbulent fluxes at the interfaces to the atmosphere and the ocean. Beyond those energy budget approaches, sea ice mass balance may also be derived from direct comparisons of sea ice growth during winter and surface and bottom melt during summer (Perovich et al., 2011b).

From various studies on the interaction of sunlight and sea ice, it was possible to improve our understanding of the effects of snow covers (Perovich et al., 2007b), melt ponds (Rösel and Kaleschke, 2012), biological interaction (Arrigo et al., 2012;Mundy et al., 2005;2007), spatial variability (Perovich et al., 2011a), and seasonal changes (Nicolaus et al., 2010a;Perovich et al., 2002;Perovich and Polashenski, 2012). But it was not yet possible to quantify large-scale, multi-seasonal, and inter-annual changes, because all these studies were limited to different regions and/or times of the year. In addition, they describe measurements on different ice types, which also differ in their optical properties as a result of their growth history (Perovich and Polashenski, 2012). One possible approach to obtain such generalized studies on the in- and under-ice energy budgets in sea-ice covered oceans would be to use a radiative transfer model in combination with surface energy budgets, as implemented by Perovich et al. (2011a). However, such a model would require adequate knowledge about the distribution of snow and sea ice (as forcing data) to derive the optical properties of sea ice and snow as function of space and time. This kind of information is not available yet, in particular not over decades. An alternative approach is to use existing remote sensing and re-analyses data together with a parameterization of light transmittance through sea ice. This method was developed by Nicolaus et al. (2012) and (2013) to calculate Arctic-wide radiation fluxes through sea ice. However, their studies were restricted to one month (August 2011), when comprehensive in-situ measurements are available from the trans-polar cruise of the German research vessel Polarstern.

In order to improve the understanding of the ongoing change in sea ice conditions and the associated impact on the partitioning of solar energy, we present a new method to quantify radiation transfer through sea ice for the entire Arctic in all seasons and for the years 1979 to 2011. Therefore, we extend and generalize the up-scaling method by Nicolaus et al. (2012) and (2013) by a new parameterization of light transmittance through various types of sea ice over the annual cycle. We also include the temporal and spatial variability of melt ponds by the application of melt-pond concentrations by Rösel et al. (2012). The timing of different seasons is derived from melt and freeze onsets from

Markus et al. (2009, updated). In order to judge the reliability of the method and to obtain a measure of uncertainty, the calculated fluxes are compared to in-situ observations in the Transpolar Drift between 86.5° and 88.5°N during the drift of the schooner Tara from April to September 2007 (Nicolaus et al., 2010a) and sensitivity studies are performed. Finally, it was possible to estimate transmitted heat fluxes through sea ice for the entire Arctic basin for the period of 1979 to 2011 as well as to derive trends.

## 2. Methods

Solar short-wave radiation fluxes (250 to 2500 nm, here also referred to as "light") through sea ice are calculated for the entire Arctic (north of 65°N) daily from 01 January 1979 to 31 December 2011. Starting from the method and parameterization by Nicolaus et al. (2012) and (2013), limited on the snow-free summer season in 2011 without any seasonal cycle of surface properties, the parameterization of light transmittance through sea ice has been extended for all seasons. Thus, transmittance is now estimated as a function of surface (snow) melt/freeze state and melt pond concentration, in addition to the previous (only) sea ice age dependence. The new parameterization was driven by satellite observations of daily sea ice concentration and surface solar irradiance to calculate fluxes as performed in Nicolaus et al. (2012) and (2013). All data sets are interpolated to a 10-km polar stereographic grid, using the nearest neighbor resampling. Although daily fluxes are calculated and available, monthly means are shown and used to discuss the findings of this study, because we aim in this extended study for seasonal changes and long-term trends.

For the main analyses we exclude open water areas as those would clearly dominate the transmitted heat flux signal. Therefore, we consider only fluxes through ice-covered areas as these are crucial for the energy and mass balance of sea ice as well as for biological processes beneath the ice cover.

## 2.1 Input data sets

The following satellite and re-analyses data sets were used (Tab. 1):

(1) Sea ice concentration was obtained from the Special Sensor Microwave Imager (SSMI/S) provided through the Ocean and Sea Ice Satellite Application Facilities (OSI SAF, product ID: OSI-401, Andersen et al. (2007)). For this study, the combination of reprocessed data (1979 to 2007) and operational data (2008 to 2011) was used. Both data sets have systematical differences due to the processing with a different set of tie point statistics for the ice concentration algorithm (Lavergne et al., 2010). However, within the documented uncertainties both data sets build the best available and consistent time series of sea ice concentration. There is no consistent uncertainty for the data product but different approaches given in Lavergne et al. (2010).

(2) For sea ice age, we used the updated data product by Maslanik et al. (2007) and (2011). It is based on ice movement satellite data calculated from different sensors and a Lagrangian feature tracking since 1979. Although this data product distinguishes the age of the ice from 1 to 10 years, here we only distinguish FYI and MYI (2 years and older), because all MYI is assumed to have similar optical properties. All data points with a sea ice concentration >0 but without sea ice age were treated as FYI. Vice versa, all data points with sea ice concentration <15% but with an age tag were treated as open water. Such modifications were necessary to obtain consistent data products from the different sources, indicating partially varying sea ice extents. The ice age data set

represents a 7-day average of either FYI or MYI without any uncertainty estimate. However, uncertainties in sea ice concentration and drift impact those values.

(3) The downward surface solar radiation was obtained four times per day from the European Centre for Medium-Range Weather Forecast (ECMWF) Era Interim re-analyses (Dee et al., 2011;Lindsay et al., 2014). The data (four values per day) were averaged to daily means and are available since 1979. Uncertainties for the data set are not reported.

(4) Sea ice surface characteristics were categorized by melt and freeze onset dates from passive microwave data (1979 to 2012) (Markus et al., 2009, updated). The data set distinguishes between the first occurrence of a melt event (early melt onset, EMO), the following continuous melt (melt onset, MO), the first occurring of freeze-up conditions (early freeze onset, EFO), and the day of persistent freezing conditions (freeze onset, FO). The standard deviations, assumed as uncertainties, for the given dates are reported as EMO ± 3.6 days, MO ± 3.7 days, EFO ± 4.5 days, and FO ± 4.0 days (Markus et al., 2009, updated).

(5) Melt pond fraction was used from Rösel et al. (2012), retrieved from MODIS sensor. As this data set is only available since 2000, melt pond fractions from 1979 to 1999 were set to constant summer mean values of 26% on FYI and 29% on MYI as given in Rösel et al. (2012) for August 2011. For consistencies with the surface characteristics, all melt pond fractions before EMO are set to zero. The mean standard deviation from 2000 to 2011, assumed as uncertainty, is calculated as ± 3%.

We do not include snow depth and sea ice thickness as input data sets, because of the lack of consistent data high temporal resolution and long-term data products. Limitations of using sea ice age as an indirect proxy for ice thickness and snow cover as well as potential other approaches for the estimation of transmitted heat fluxes are discussed below.

**2.2 Solar heat flux equations**

Solar heat input through sea ice into the ocean ($E_T(t,x,y)$) is calculated as the product of the downward solar radiation ($E_d$), the sea ice concentration ($C_i$), and the total transmittance of pond covered sea ice ($\tau_i$) for each grid cell for each day from 01 January 1979 to 31 December 1999:

$$E_T(t,x,y) = E_d(t,x,y) \cdot C_i(t,x,y) \cdot \tau_i \qquad \textbf{(1)}$$

with time t and position (x,y).

Since 01 January 2000, when satellite derived melt-pond concentrations are available, the solar heat input through sea ice into the ocean ($E_T$) is calculated as the sum of fluxes through bare ice ($E_B$) and melt ponds ($E_P$):

$$E_T(t,x,y) = E_B(t,x,y) + E_P(t,x,y)$$

$$E_T(t,x,y) = E_d(t,x,y) \cdot C_i(t,x,y) \cdot \left[1 - C_p(t,x,y)\right] \cdot \tau_b(t,x,y) + E_d(t,x,y) \cdot C_i(t,x,y) \cdot C_p(t,x,y) \cdot \tau_p(t,x,y) \qquad \textbf{(2)}$$

with the transmitted solar radiation at the bottom of the ice $E_T$, downward solar radiation $E_d$, sea ice concentration $C_i$, melt pond fraction $C_p$, transmittance of bare sea ice $\tau_b$, transmittance of melt ponds $\tau_p$, time t and grid cell (x,y).

To obtain the total solar heat input per unit area for a certain time period ($Q_T(x,y)$), the heat flux is calculated for each grid cell and then integrated over the given time ($\Delta t$)

$$Q_T(x,y) = \sum E_T(t,x,y)\,\Delta t. \qquad \textbf{(3)}$$

Spatial integration over the entire Arctic Ocean (north of 65°N), reveals the Arctic-wide total solar heat input $Q_T$.

Assuming a sea ice density $\rho_{ice}$ of 917 kg m$^{-3}$, a latent heat of fusion $L_{ice}$ of 0.3335 J kg$^{-1}$, and in addition no changes in longwave, latent, and conductive heat fluxes as well as the sea ice being at its melting point, $Q_T(x,y)$ can be converted into sea ice melt rate $m_{eq}$:

$$m_{eq} = \frac{Q_T(x,y)}{L_{melt} \cdot \rho_{ice}}. \qquad \textbf{(4)}$$

## 2.3 Seasonality of surface properties and transmittance of Arctic sea ice

To calculate solar heat fluxes under Arctic sea ice for an entire year, the main challenge is to parameterize the seasonal evolution of $\tau_b(t,x,y)$. This is mainly achieved by merging the sea-ice age information (Maslanik et al., 2007;2011) with the melt/freeze status (Markus et al., 2009, updated) into six surface types.

### 2.3.1 Definition of sea ice types

Figure 1 shows the annual cycle of these six sea ice classes together with surface properties of Arctic sea ice. Those classes are introduced to avoid abrupt changes in the optical properties during the transition from spring to summer as well as from summer to fall. After EMO, *melting FYI* and *melting MYI* are introduced for sea ice completely melting during the summer melt. Therefore, it is necessary to classify for each cell whether it is becoming ice free (sea ice concentration less than 15%) or not. To do so, the ice concentration of each pixel is evaluated for all days until EFO. If the pixel becomes ice free, the last day of melting is stored for later calculations. According to Maslanik et al. (2007) and (2011), *FYI* surviving the summer melt turns into *MYI* after week 36 of the year. As the immediate change in ice age tagging is not associated with an immediate change in sea ice properties, we include an additional class of *new MYI*. It turns finally into *MYI* at the end of the year. As soon as sea ice concentration is getting higher than 15% *new FYI* is formed.

In the following, the composition of bare sea ice and melt ponds is called pond covered sea ice.

**2.3.2 Transmittance of pond covered sea ice**

The seasonal evolution of surface properties and transmittance of Arctic sea ice is divided into six different phases (note the difference of ice types and seasonal phases). The timing of these phases is based on the melt and freeze onset data set by Markus et al. (2009, updated). Our parameterization of seasonal variations of light transmittance considers the transmission through both sea ice and snow and is mostly based on results of two field campaigns focusing the understanding of ice-ocean-atmosphere processes that control the partitioning of solar radiation among reflection, absorption and transmittance: The Surface Heat Budget of the Arctic Ocean experiment (SHEBA) from 1997 to 1998 (Perovich, 2005) and measurements on MYI in the Transpolar Drift between 86.5° and 88.5°N during the drift of the schooner Tara from April to September 2007 (Nicolaus et al., 2010a). In addition, analyses from previous observations by Perovich (1996), Perovich et al. (1998), and Nicolaus et al. (2010b) are used. Figure 2a shows the seasonal total transmittance of pond covered sea ice ($\tau_i$) for constant pond concentrations of 26 and 29 % for FYI and MYI, as it was used from 1979 to 2000. This composition of a given mixture of ponds and bare ice was used to develop the seasonal cycle of transmittance, as described in the next paragraphs. All transmittances of the different phases are compiled in Table 2.

*Phase I: Winter (from FO+60 days to EMO)*

Winter conditions are characterized by snow covered sea ice without melt ponds. The snow cover is assumed to be cold, dry and optically thick. It determines the optical properties. Thus, radiative fluxes through sea ice are small. The best available transmittance observations for such conditions are those measured during the first days of the Tara drift, although it was early April already. Hence transmittance was accordingly set to 0.002 (Nicolaus et al., 2010a).

*Phase II: Early melt (from EMO to MO)*

EMO denotes the first significant change in optical properties. Snow depth decreases whereas temperatures of the surface and sea ice increase. Consequently, snow is no longer optically thick and is getting wet and first melt ponds might occur. Here we assume a linear increase of $\tau_i$ until MO.

Nicolaus et al. (2010a) calculated a transmittance of 0.02 for MYI for the day of MO. Beyond, Perovich and Polashenski (2012) reveal that the surface albedo of FYI is about half that of MYI at the same time. Adapting this albedo evolution to the transmittance, the transmittance of FYI is assumed as 0.04 at MO.

*Melting FYI and melting MYI*

After EMO, it is considered that the annual melt of snow and sea ice strongly impacts light transmittance. It is assumed that the optical properties of melting sea ice differ for both ice types. Thus, melting FYI and melting MYI are separated in the parameterization of $\tau_i$.

In order to describe these classes, laboratory studies by Perovich (1996) on the albedo evolution during the initial ice growth phase were applied to the transmittance evolution assuming an inverse behavior. Therefore, the increase in transmittance of seasonal sea ice at the aggregate scale can be described as roughly exponential (Perovich, 1996). Assuming the transmittance transition from melting sea ice to open ocean inverse of the albedo transition (Perovich, 1996), we use a transmittance of 0.4 for the last existing sea ice. Thus, an exponential increase between EMO and the last day of melting for the according pixel is fitted.

*Phase III: Continuous melt (from MO to MO+14 days)*

After MO, snow is assumed to melt completely within 14 days (Nicolaus et al., 2006) and pond cover fraction increases rapidly until the maximum pond cover is reached at the end of this phase (Nicolaus et al., 2010a). The transmittance continues increasing linearly until begin of summer (MO+14 days).

*Phase IV: Summer (from MO+14 days to EFO)*

During this phase the sea ice surface is characterized by strong sea ice melt and culminates in the minimum ice concentration of each pixel. The surface consists of a mixture of bare ice and melt ponds with comparably small changes. Hence, $\tau_i$ is assumed to be constant for sea ice that survives summer melt. Based on observed transmittances of solar radiation through FYI and MYI during TransArc 2011 (Nicolaus et al., 2012), we use summer transmittances of 0.04 of bare FYI, 0.01 of bare MYI, 0.087 of pond covered FYI, and 0.05 of pond covered MYI. Those numbers are then weighted with melt pond fractions (Rösel and Kaleschke, 2012).

*Phase V: Fall freeze-up (from EFO to FO)*

Air and surface temperatures drop below 0°C resulting in first surface freezing. Subsequently, snow accumulation may start and former melt ponds refreeze but may still be recognized through the new snow cover. Thus, the transmittance is decreasing rapidly. In analogy to Phase III the transmittance of FYI decreases to 0.04 and for MYI to 0.02 until FO. Additionally, sea ice that survived the summer melt is promoted to one-year-older ice in week 36/37 according to Maslanik et al. (2007) and new ice forms. The transmittance of new first year ice evolves correspondingly to the melting sea ice surface, described above. From EFO until the begin of winter (FO+60 days) the strong growth of sea ice, increasing sea ice thickness, results in an exponential decrease in light transmission through newly formed FYI.

*Phase VI: Continuous freeze (from FO to FO+60 days)*

Continuous freezing and an increasing snow accumulation towards an optically thick snow layer and the gradual disappearance of melt ponds characterize this phase. Beyond new sea ice formation, the existing sea ice is getting thicker and older and deformation is increasing. The transmittance is decreasing back to 0.02 until winter. It is assumed that at the end of the freezing phase (FO+60 days) the surface properties of all newly formed FYI can be considered as equivalent. Afterwards, the accumulated optically thick snow layer dominates the optical properties of FYI and MYI again (Phase I).

### 2.3.3 Transmittance of bare ice and ponds

After 2000, when melt pond products are available from Rösel and Kaleschke (2012), the transmittances of bare ice ($\tau_b$) and ponds ($\tau_p$) are treated separately (Figure 2b). The modal transmittance of melt ponds is constant over the entire melt season. It is set to 0.22 for FYI and 0.15 for MYI, as measured during TransArc 2011 (Nicolaus et al., 2012).

The seasonal evolution of transmittance of bare ice ($\tau_b$) follows the transmittance for pond covered sea ice ($\tau_i$):

$$\tau_b(x,y) = \tau_i(x,y) \cdot \frac{\tau_b(summer,x,y)}{\tau_i(summer,x,y)} \quad \textbf{(4)}$$

The values of $\tau_b$(summer,x,y) and $\tau_i$(summer,x,y) are the constant values during summer as given in Table 2. Thus, the ratio of both is constant for MYI (0.20) and FYI (0.46). Finally, those transmittances are scaled with the pond concentration, as given in Equation 2.

### 2.4 Deriving trends

Based on the results of our calculations of the solar heat input through sea ice into the ocean, trends are analyzed from 1979 to 2011. The trends (monthly and annual) are calculated by a linear least-squares fit of the total mean (monthly or annual) heat flux for each grid cell ($Q_T$(x,y)). In order to exclude artifacts of changes in sea ice concentration, all trends in transmittance were normalized based on the trends in sea ice concentration. All trends were calculated for both the annual mean ice covered area in 2011 and the monthly mean covered area in 2011 (sea ice concentration > 15%) to allow for a representative comparison. Regions that were not ice covered at any time in 2011 are excluded from the main analysis and discussion.

## 3. Results

### 3.1 Seasonal cycle of solar radiation under Arctic sea ice in 2011

Based on the availability of all input data sets and the seasonality of transmittances, the solar heat input through sea ice into the ocean is analyzed from 1979 to 2011. Figure 3 shows the monthly mean heat input ($Q_T$(x,y), Equation 3) under Arctic sea ice (ice covered areas only) from April to September 2011. The example of 2011 was selected to ease later comparisons with the previous results for August 2011 by Nicolaus et al. (2012) and (2013). From October to March the monthly mean solar radiation under sea ice was smaller than $0.2\times10^5$ $Jm^{-2}$ with an Arctic-wide total under-ice heat flux ($Q_T$) of up to $0.4\times10^{19}$ J. Since this represents less than 1% of the annual Arctic-wide heat flux of $53.3\times10^{19}$ J (Equation 3), those months are neglected for further analyses and discussion. In April the mean heat flux increased to $0.4\times10^5$ $Jm^{-2}$ with a maximum of 7 to $8\times10^5$ $Jm^{-2}$, representing an equivalent mean ice melt of 7 to 8 cm per month (Equation 4) in the marginal ice zone East of Spitsbergen. The transmittance triples from 0.005 in April to 0.015 in May, and together with increasing surface fluxes, the $Q_T(x,y)$ increased from $1.0\times10^{19}$ J to $5.5\times10^{19}$ J during this time. The Barents Sea showed averaged transmitted heat fluxes up to $25\times10^5$ $Jm^{-2}$ with a mean of $2.2\times10^5$ $Jm^{-2}$ in May. Thus, the maximum equivalent sea ice melt was 25 cm for May 2011. From May to June, the most pronounced monthly increase was found for $Q_T(x,y)$ (to $9.3\times10^5$ $Jm^{-2}$) and the transmittance (0.054). The maximum $Q_T(x,y)$ was about $30\times10^5$ $Jm^{-2}$, also shown in an maximum melt rate of about 30 cm per month. June was the month of the highest $Q_T$ ($20.9\times10^{19}$ J) associated with the highest solar surface irradiance over the entire Arctic Ocean ($851\times10^{19}$ J). That increase was linked with the beginning of the melt phase (mean MO on 30 May 2011) and the associated strong snow melt. During this time, the difference between thin melting sea ice on the sea ice edge and the persistent sea ice cover became most obvious, e.g. in the Chuckchi and Beaufort Seas. In July, the Arctic wide average of $Q_T(x,y)$ reached its annual maximum of $9.8\times10^5$ $Jm^{-2}$. This resulted mainly from the annual maximum in mean transmittance of 0.089, and lead to a monthly flux $Q_T$ of $18.4\times10^{19}$ J. The impact of the different optical properties ($\tau_i$) of MYI and FYI become most obvious in July, because the difference of both values is at its maximum. Also the strong decrease of sea ice concentration along the ice edge becomes more important for the under-ice heat fluxes, because light transmittance increases strongly in these regions. The August decrease of $Q_T(x,y)$ by more than 50% to $4.4\times10^5$ $Jm^{-2}$ along with only a slight reduction of transmittance to 0.084 is mainly caused by the strong decrease in solar surface irradiance ($679\times10^{19}$ J). These surface fluxes are only half of those during the previous months. Maximum $Q_T(x,y)$ reached up to $19\times10^5$ $Jm^{-2}$. In September the $Q_T(x,y)$ decreased further to $0.6\times10^5$ $Jm^{-2}$ related to a low transmittance of 0.039 and $Q_T$ was $0.7\times10^{19}$ J.

### 3.2 Light transmission from 1979 to 2011

The new data set of $Q_T(x,y)$ allows quantification of annual budgets, regional differences, and decadal trends. Figure 4a illustrates the strong regional variability of the total solar heat input through sea ice into the ocean ($Q_T(x,y)$) ranging from 20 to 100 $MJm^{-2}$ for the given period. This range in heat fluxes is equivalent to an ice melt rate of 24 to 120 m per year. The mean total solar heat input per grid cell in the area of the mean sea ice extent was 46 $MJm^{-2}$.The maximum $Q_T(x,y)$ occurs at the edge of the marginal ice zone in the Canadian Arctic Archipelago (up to 110 $MJm^{-2}$/130 cm melt per year) and the East Siberian Sea and Chukchi Sea (up to 80 $MJm^{-2}$/94 cm melt per year). In contrast, excluding ice edge effects, the minimum $Q_T(x,y)$ was found in the Central Arctic, a MYI dominated region of low transmittance.

The mean trend of $Q_T(x,y)$ was 1.5 $\%a^{-1}$ (excluding sea ice edge effects) with a maximum of +4 $\%a^{-1}$ in the East Siberian Sea and southern part of the North American and Russian Arctic Basin (Figures 4b and 5a). This trend translates into an increase of the potential sea ice melt of 63% over the observation period of 33 years. The reason is likely the prolongation of the melt season in these regions. According to a linear regression from

1979 to 2011 for the entire Arctic, the mean MO was 4 days earlier, shifting from day 145 (24 May) to day 141 (20 May). The strongest trend of $4.8\times10^{18}$ J $a^{-1}$ was found for June followed by May and July with $1.8\times10^{18}$ J $a^{-1}$. August shows a comparably weak negative trend of $-0.2\times10^{18}$ J $a^{-1}$. Assuming an identical sea ice extent in 1979 and 2011, the increase in the annual mean solar heat flux through sea ice ($Q_T$) amounts to $22.5\times10^{19}$ J in the Arctic over the entire period. This means an averaged increase by 33%. Over all, 94% of the total annual solar heat input through Arctic sea ice was observed during the four key months: May to August. Furthermore, heat flux time series (annual, June, July) show an increasing variability after 1999.

# 4. Discussion

## 4.1 Seasonality and trends of transmitted fluxes

The total annual solar radiation under Arctic sea ice amounted to $53.3\times10^{19}$ J in 2011. Based on this, May to August are the most important months for the radiative energy partitioning. During this time, 96% ($51.2\times10^{19}$ J) of the total annual solar heat input is transmitted through the sea ice. Including April and September in addition, 99% ($52.9\times10^{19}$ J) of the total annual flux is transmitted, within only one third of the year. Generalizing the monthly fluxes, the annual cycle may be summarized in three phases: (1) The heat input through snow and sea ice into the ocean is negligible between October and March, (2) solar surface radiation dominates the under-ice light conditions from April to June, because transmittance increases only slowly, while surface irradiance determines most of the observed changes and variability, (3) during summer (July to September), energy fluxes depend mainly on the sea ice type, showing large differences in transmittance between FYI and MYI.

Comparing our results to the development of the solar heat input into the ice presented by Perovich et al. (2011a, Fig. 2), both the solar heat input to the upper ocean and the solar heat input to the sea ice demonstrate a positive annual trend of 1 to 1.5% per year during the last decades. The increasing energy in the ice and upper ocean might both lead to a stronger sea ice melt. Therefore, the radiative heating of the upper ocean might contribute to a higher conductive ocean heat flux to the ice. This increase in bottom and internal melt is affecting the sea ice mass balance. An increasing light absorption of Arctic sea ice due to more seasonal and less multi year ice was also found by Nicolaus et al. (2012).

The trend towards more light transmission through sea ice, does not only impact the light conditions right at the bottom of the sea ice, but also affects the horizontal and vertical light field in the ice covered ocean. More light at the bottom of sea ice will deepen the euphotic zone, as more light penetrates deeper into the ocean (Frey et al., 2011;Katlein et al., 2014). It contributes to an increase in mixed layer temperature, and provides more energy for primary production and biogeochemical processes in and beneath the sea ice. However, it has to be noted that an increase in light availability does not necessarily increase biological activity, but might also be harmful (Leu et al., 2010).
However, an increase in transmittance will accelerate internal and bottom melt, which in turn will reduce the thickness of sea ice and increase transmittance. That feedback process can be trigger a transmittance-melt feedback.

Our calculated trends are based on constant pond fractions before 2000. Speculation of even greater pond coverage might even increase the trends. The increasing melt pond fraction on Arctic sea ice between 2000 and 2011 has been also shown in Rösel and Kaleschke (2012).

All findings are based on trend estimates that were normalized for the trend in sea ice concentration (section 2.4). However, to point towards the future importance of such heat fluxes, it is important to consider that those sea ice concentration trends differ significantly for different months. While the trend is -0.1% $a^{-1}$ for September, it is only -0.06% $a^{-1}$ for June, the months when the largest impact on absolute fluxes is observed. In April and May, when the most significant relative changes are observed, and when the impact for biological primary production is expected increase crucially (Wassmann and Reigstad, 2011), the trend in sea ice concentration is even positive with +0.04% $a^{-1}$ Including the ice concentration effect, and thus, including the direct heat input to the open ocean, results in an annual trend of ±1.1% $a^{-1}$ compared to +1.5% $a^{-1}$ with the normalized trend. The negative trend in the open ocean heat input is evident in areas of ice motion causing an increase in ice concentration as also shown in Perovich et al. (2007a, 2011a). This comparison emphasizes the dominance of the albedo feedback mechanism and the strong influence of the trend in sea ice concentration on the heat budget of the entire system.

**4.2 Validation**

A validation for the calculated trends and spatial variability is almost impossible as insufficient field data with adequate spatial and temporal coverage are available. However, some comparisons with time series of light transmission from different field studies may be performed to identify major uncertainties.

Here we compare, surface and transmitted solar irradiance of the presented method with in-situ measurements during the Transpolar Drift of Tara from 29 April to 28 August 2007 (Nicolaus et al., 2010a). Nearest-neighbor grid points within 0.5° of the daily Tara position were extracted from the presented data set and averaged. Figure 6a (red and green lines) shows a comparison of the time series of transmitted solar irradiance from both data sets. Until 08 June, the transmitted solar irradiance under sea ice varies only little around 0.5 $Wm^{-2}$ for both, the calculated and the measured time series. Afterwards until end of June, the measured transmitted fluxes increased steadily towards 10 $Wm^{-2}$, whereas calculated fluxes were highly variable with most values below 4 $Wm^{-2}$. Hence, the total solar heat input through the sea ice to the ocean from 1 May to 16 July 2007 was 21.4 $MJm^{-2}$ for the observed Tara data, whereas the calculated data resulted in a 17% lower total heat flux of 17.7 $MJm^{-2}$. The calculated underestimation equals 1 cm of sea ice melt for this period. During summer (16 July to 14 August), under-ice fluxes cannot be compared reasonably since the sensor at Tara was strongly influenced by biological processes, causing an increased absorption and reduced transmitted fluxes. Thus, the calculated fluxes were overestimated by 11.6 $MJm^{-2}$, representing an equivalent sea ice melt of 4 cm during summer.

After 14 August, the measured transmitted heat flux increased rapidly to about 6 $Wm^{-2}$, comparable to the calculated one. Finally, the decrease in solar elevation caused decreasing transmitted fluxes in both data sets, resulting in similar heat fluxes of $0.28\times10^{3}$ $MJm^{-2}$ after 14 August.

Main reason for these differences is the timing of the phases describing the surface characteristics. While both data sets have a coincident EMO on 09 June, large differences are evident for the later phase transitions: The observed MO at Tara was on 21 June whereas the calculated MO for the center position was 17 days later on 8 July. Taking also the other 8 neighbors in account, mean MO was on 13 June. This shows that there is a difference of 25 days in MO on the 10 km grid. As presented above, the transmitted heat flux strongly depends on the timing of the different melt phases by Markus et al. (2009). EFO was observed on 15 August during Tara, whereas the satellite data maintains summer melt conditions until 14 September. However, the total solar heat input through sea ice was similar for both data sets. Thus, the solar radiation flux under Arctic sea ice strongly depends on the timing of EMO and MO, while the timing of EFO and FO seems to be of less importance since the begin of the melt season coincides with maximal surface solar heat fluxes. The timing of melt onset has also a large influence on the total amount of light absorption, as shown in Stroeve et al. (2014). Consider the ongoing lengthening of the melt season by up to two weeks per decade (by a later EMO), their calculations suggest an albedo decrease of 9% per decade.

In a second validation step, the heat fluxes were re-calculated using the onset dates as observed during Tara instead of those by Markus et al. (2009) (Figure 6, black lines). This eliminated the impact of the onset dates on the results. Nevertheless, the calculated total solar heat input through sea ice was still differing by 18% (25.4 $MJm^{-2}$) from the Tara fluxes until 16 July (Figure 6a) due to an unexpected peak in $Q_T(x,y)$ in July. In addition, the calculated time series showed still a large day-to-day variability, including much higher transmittances than observed at Tara. The main reason for this is the alternation of sea ice types (FYI and MYI), whereas the Tara floe consisted of MYI only. Consequently, the strong differences in optical properties of FYI and MYI, as parameterized here, strongly contribute to the overall energy budget. To overcome this problem, FYI/MYI fractions per grid cell (Kwok, 2004) could be used instead of the presented discrete distinction. However, such a data set is not yet available for the given time span.

Hudson et al. (2013) measured heat fluxes and calculated transmittances of Arctic FYI in July/August 2012. However, a direct comparison of energy fluxes, as for the Tara measurements, is not possible, because the melt-pond concentration data set ends in December 2011. August transmittance in our study (0.087) is based on the observations by Nicolaus et al. (2012), which is only half of the 0.16 found by Hudson et al. (2013). Hence, it may be assumed that heat fluxes through sea ice would be larger based on those measurements. Differences between both studies mainly result from differences in sea ice thickness during the respective campaigns as well as the different methods of quantifying transmittance (mean value vs. modal value) (Hudson et al., 2013).

Measurements from Ice-Tethered Profilers (ITPs) (Krishfield et al., 2008) could be used as an alternative approach to estimate uncertainties of the new parameterization. They allow quantifying the heat content of the uppermost ocean and its changes. However, such comparison would require a significant extension of the presented study, integrating radiation fluxes to larger depths and through open water. Similarly, the inclusion of a radiation transfer model is beyond the aim of this study. The advantage of this study is the rather simplistic approach based on a seasonal parameterization of under-ice fluxes applied to existing large-scale data products.

An improvement of this study would be the inclusion of sea ice thickness (e.g. CryoSat-2, IceSat, OperationIceBridge) and snow depth (e.g. AMSR-E) observations from satellites. As all other input data, those products need to be consistent over many years and reliable during all seasons. But this is not the case yet, and even latest data sets have huge uncertainties or are not available after melt onset (e.g. Ricker et al. (2014)), which is the most important time with respect to transmitted heat fluxes. Hence these parameters are not applicable for such parameterizations yet. Instead, sea ice age is used as a proxy for ice thickness and snow depth distribution. It also includes information about roughness and deformation of the sea ice surface. These characteristics are crucial for the description of optical properties of sea ice.

Including a seasonal cycle for the transmittance of melt ponds on FYI and MYI would also improve the presented heat flux calculations. The additional uncertainty due to this lack is assumed as comparable low as the applied transmittances represent the transmittance distribution of different pond depths [Nicolaus et al., 2012]. The main uncertainty is expected in the beginning of the melt season due to partial frozen melt ponds. This is considered by the uncertainties of the timing of the melt season, which is discussed below.

### 4.3 Sensitivity studies

Based on uncertainties of the independent input variables (timing and length of the melt season, ice age, melt pond fraction) several sensitivity studies have been performed to estimate the uncertainty for the presented parameterization.

The first study alters the timing and length of the melt season on the solar heat input to the upper ocean. Three cases are discussed: shifting the melt season dates by (Case 1a) the averaged uncertainty of 4 days as given by (Markus et al., 2009), (Case 1b) 7 days due to on the available ice age data once per week (Maslanik et al., 2011), and (Case 1c) (averaged) 14 days as derived from comparisons with the Tara field data (Nicolaus et al., 2010a). Based on the observed ongoing trend towards a lengthening of the melt season, all sensitivity studies were only performed for earlier EMO and MO, and a later EFO and FO exemplarily for 2011.

Extending the melt season by 4 days (Case 1a) results in Arctic-wide mean EMO on 12 May and MO on 27 May. This affects for most regions a time of high sea ice concentration and large solar surface irradiance. It results in an increase in total annual solar heat input through sea ice to the ocean ($Q_T$) of 7% from $53.3 \times 10^{19}$ J to $57.0 \times 10^{19}$ J for the entire year 2011. The strongest increase of 20 % compared to the reference melt onset dates was found for May, while the strongest absolute increase of $1.9 \times 10^{19}$ J was found in June.

A 7 days earlier (Case 1b) EMO (8 May) and MO (23 May) results in an additional heat amount of $5.9 \times 10^{19}$ J (+11%) compared to the reference system for the total annual heat input to the upper ocean. Shifting the melt season another 7 days (Case 1c) backwards (1 May and 16 May), the increase in $Q_T$ is more than double compared to the 7-day-shift (Tab. 3, $66.3 \times 10^{19}$ J). The pronounced increase is most evident in May, when 90% more light transmission was found than in the reference system. The strongest absolute increase of $6.2 \times 10^{19}$ J (transmittance from 0.054 to 0.067) was derived for June. The spatial distribution of the impact of the 14 days earlier EMO and MO showed the largest increase of solar heat input to the upper ocean in the marginal ice zone, adding up to more than 100% (Figure 7a).

Extending the melt season by 14 days (Case 1c) later EFO and FO (21 October and 2 November), results in a 1% increase of $Q_T$ from $53.3 \times 10^{19}$ J to $53.9 \times 10^{19}$ J (Fig. 7b). Since the surface solar radiation is much less than between April and June, the change in the end of the melt season affects only parts of August and September (increase of 9% from

$7.02\times10^{19}$ J to $7.65\times10^{19}$ J). A 7 day or rather 4 day (Cases 1a and 1b) later EFO and FO have a negligible effect on the total annual transmitted heat flux of less than 1%.

In a second sensitivity study, the influence of the ice type was quantified. As the sea ice type data contain no uncertainty, the study is based on the ongoing discussion towards an only FYI-covered Arctic sea ice area. The reference ice cover of 2011 consists of 56% FYI and 44% MYI in August 2011. Assuming that all sea ice in 2011 was MYI, the mean transmitted flux decreased by 34 % to $35.5\times10^{19}$ J. In contrast, assuming that only FYI was present increased that value by 18 % to $62.7 \times10^{19}$ J. Hence, the transition from a MYI to FYI dominated Arctic sea ice regime results in a further increase of solar heat flux under Arctic sea ice.

The third sensitivity study investigates the effects of melt pond fraction uncertainties. Here we consider two cases: (Case 3a) Rösel et al. (2012) give a mean uncertainty of 3% and (Case 3b) we estimate an uncertainty of 20% due to the neglected seasonal cycle. Adapting these assumptions, an increasing melt pond fraction of 3 % (20%) results in an increase of the transmitted heat flux of 1 % (9%).

Uncertainties in the solar surface radiation and sea ice concentration are not analyzed through additional sensitivity studies, because they impact the results linearly (Equation 2).

## 5 Summary and conclusions

The new parameterization for light transmission through Arctic sea ice in combination with time series derived from satellite observations and re-analyses allows to quantify solar short-wave radiation fluxes through Arctic sea ice for the entire annual cycle over 33 years (1979 to 2011). Therefore, highest fluxes were calculated for June. The presented results suggest that 96% of the total annual solar heat input through sea ice occur in only 4 months (May to August). Regarding the time period from 1979 to 2011, an increase in light transmission of 1.5%/year with regional maxima of 4.0% is found. Hence, the amount of short-wave radiation that may contribute to sea ice bottom melt has increased by 63% over these 33 years. The results of our sensitivity studies show that energy fluxes strongly depend on the timing of melt onset, sea ice types (first and multi year ice), and melt pond fraction. Those parameters are the most critical ones for the shown calculations and describe the most critical uncertainties. The calculated trends are affected most of these uncertainties.

All these results consider the fluxes through ice-covered ocean only, which highlights that changes in sea ice properties have a large impact on the energy budget and should not be neglected compared to the obvious effect of sea ice retreat. However, the ongoing retreat of sea ice will cause additional increases in radiation fluxes into the Arctic Ocean. The access heat will also contribute to an increase of heat stored in the ocean mixed layer and will impact the melt season duration and timing, particularly autumn refreezing.

A comparison with trends of solar heat fluxes into the sea ice by Perovich et al. (2011a) suggests an equal increase in transmitted and absorbed energy. This additional energy input into the sea ice and the upper ocean would also impact inner sea ice structures as well as internal and basal melting.

More investigations of bio-geo-physical connections will be needed to better quantify the effects of the changing physical environment on the ecosystem and element cycles, and vice versa. Additional work will also be needed to improve Arctic-wide snow depth and sea ice thickness data products. Those products should on a good description of surface properties during the spring-summer-transition, when the largest uncertainties were found. Such time series might become available from new data products merging observations from different satellites and sensor types (e.g. SMOS, CryoSat-2, AMSR-E), and potentially also numerical models. The non-existence of such reliable long-term and Arctic-wide data sets was the main reason to develop the presented method, based on available parameters. Otherwise, the application of a radiation transfer model with adequate input (forcing) data would have been an obvious alternative.

**Acknowledgements**

We are most grateful to Jim Maslanik (University of Colorado Boulder), Thorsten Markus and Jeffrey Miller (both NASA Goddard Space Flight Center), Thomas Lavergne (OSISAF, Met Norway), and Anja Rösel and Larsch Kaleschke (both University of Hamburg) for data provision and support through manifold discussions on their data products and processing details. We thank Christian Katlein (Alfred-Wegener-Institut Helmholtz-Zentrum für Polar- und Meeresforschung) and Martin Claussen (Max Planck Institute for Meteorology) for constructive comments on the manuscript. We appreciate the efforts of the two anonymous reviewers and the scientific editor in improving the manuscript. The study was funded through the Remote Sensing Alliance of the Helmholtz Association and the Alfred-Wegener-Institut Helmholtz-Zentrum für Polar- und Meeresforschung.

**References**

Andersen, S., Breivik, L. A., Eastwood, S., Godøy, Ø., Lind, M., Porcires, M., and Schyberg, H.: OSI SAF Sea Ice Product Manual,v3. 5, EUMETSAT OSI SAF,Ocean and Sea Ice Sattelite Application Facility, Tech. Rep. SAF/OSI/met. no/TEC/MA/125, 2007.

Arrigo, K. R., Perovich, D. K., Pickart, R. S., Brown, Z. W., van Dijken, G. L., Lowry, K. E., Mills, M. M., Palmer, M. A., Balch, W. M., Bahr, F., Bates, N. R., Benitez-Nelson, C., Bowler, B., Brownlee, E., Ehn, J. K., Frey, K. E., Garley, R., Laney, S. R., Lubelczyk, L., Mathis, J., Matsuoka, A., Mitchell, B. G., Moore, G. W. K., Ortega-Retuerta, E., Pal, S., Polashenski, C. M., Reynolds, R. A., Schieber, B., Sosik, H. M., Stephens, M., and Swift, J. H.: Massive Phytoplankton Blooms Under Arctic Sea Ice, Science, 336, 1408-1408, Doi 10.1126/Science.1215065, 2012.

Comiso, J. C.: Large decadal decline of the Arctic multiyear ice cover, Journal of Climate, 25, 1176-1193, 2012.

Deal, C., Jin, M. B., Elliott, S., Hunke, E., Maltrud, M., and Jeffery, N.: Large-scale modeling of primary production and ice algal biomass within arctic sea ice in 1992, Journal of Geophysical Research-Oceans, 116, Artn C07004
Doi 10.1029/2010jc006409, 2011.

Dee, D. P., Uppala, S. M., Simmons, A. J., Berrisford, P., Poli, P., Kobayashi, S., Andrae, U., Balmaseda, M. A., Balsamo, G., and Bauer, P.: The ERA‐Interim reanalysis: Configuration and performance of the data assimilation system, Quarterly Journal of the Royal Meteorological Society, 137, 553-597, 2011.

Frey, K. E., Perovich, D. K., and Light, B.: The spatial distribution of solar radiation under a melting Arctic sea ice cover, Geophysical Research Letters, 38, Artn L22501
Doi 10.1029/2011gl049421, 2011.

Grenfell, T. C., Light, B., and Perovich, D. K.: Spectral transmission and implications for the partitioning of shortwave radiation in arctic sea ice, Annals of Glaciology, 44, 1-6, 2006.

Haas, C., Pfaffling, A., Hendricks, S., Rabenstein, L., Etienne, J. L., and Rigor, I.: Reduced ice thickness in Arctic Transpolar Drift favors rapid ice retreat, Geophysical Research Letters, 35, 10.1029/2008gl034457, 2008.

Hudson, S. R., Granskog, M. A., Sundfjord, A., Randelhoff, A., Renner, A. H. H., and Divine, D. V.: Energy budget of first-year Arctic sea ice in advanced stages of melt, Geophysical Research Letters, 40, 2679-2683, Doi 10.1002/Grl.50517, 2013.

Katlein, C., Nicolaus, M., and Petrich, C.: The anisotropic scattering coefficient of sea ice, Journal of Geophysical Research-Oceans, 119, 842-855, Doi 10.1002/2013jc009502, 2014.

Krishfield, R., Toole, J., Proshutinsky, A., and Timmermans, M. L.: Automated Ice-Tethered Profilers for Seawater Observations under Pack Ice in All Seasons, J Atmos Ocean Tech, 25, 2091-2105, Doi 10.1175/2008jtecho587.1, 2008.

Kwok, R.: Annual cycles of multiyear sea ice coverage of the Arctic Ocean: 1999–2003, Journal of Geophysical Research, 109, C11004, 10.1029/2003JC002238, 2004.

Lavergne, T., Killie, M. A., Eastwood, S., and Breivik, L.-A.: Extending the CryoClim Arctic sea ice extent time series with operational OSI SAF products from 2008 onwards, Norwegian Meteorological Institute note, 7, 2010.

Leu, E., Wiktor, J., Soreide, J. E., Berge, J., and Falk-Petersen, S.: Increased irradiance reduces food quality of sea ice algae, Marine Ecology Progress Series, 411, 49-60, Doi 10.3354/Meps08647, 2010.

Light, B., Grenfell, T. C., and Perovich, D. K.: Transmission and absorption of solar radiation by Arctic sea ice during the melt season, Journal of Geophysical Research: Oceans (1978,Äì2012), 113, 2008.

Lindsay, R., Wensnahan, M., Schweiger, A., and Zhang, J.: Evaluation of Seven Different Atmospheric Reanalysis Products in the Arctic*, Journal of Climate, 27, 2588-2606, Doi 10.1175/Jcli-D-13-00014.1, 2014.

Markus, T., Stroeve, J. C., and Miller, J. A.: Recent changes in Arctic sea ice melt onset, freezeup, and melt season length, Journal of Geophysical Research, 114, C12024, Artn C12024
Doi 10.1029/2009jc005436, 2009.

Maslanik, J., Stroeve, J., Fowler, C., and Emery, W.: Distribution and trends in Arctic sea ice age through spring 2011, Geophysical Research Letters, 38, Artn L13502
Doi 10.1029/2011gl047735, 2011.

Maslanik, J. A., Fowler, C., Stroeve, J., Drobot, S., Zwally, J., Yi, D., and Emery, W.: A younger, thinner Arctic ice cover: Increased potential for rapid, extensive sea-ice loss, Geophysical Research Letters, 34, Artn L24501
Doi 10.1029/2007gl032043, 2007.

Mundy, C. J., Barber, D. G., and Michel, C.: Variability of snow and ice thermal, physical and optical properties pertinent to sea ice algae biomass during spring, J Marine Syst, 58, 107-120, Doi 10.1016/J.Jmarsys.2005.07.003, 2005.

Mundy, C. J., Ehn, J. K., Barber, D. G., and Michel, C.: Influence of snow cover and algae on the spectral dependence of transmitted irradiance through Arctic landfast first-year sea ice, Journal of Geophysical Research-Oceans, 112, Artn C03007
Doi 10.1029/2006jc003683, 2007.

Nicolaus, M., Haas, C., Bareiss, J., and Willmes, S.: A model study of differences of snow thinning on Arctic and Antarctic first-year sea ice during spring and summer, Annals of Glaciology, 44, 147-153, 2006.

Nicolaus, M., Gerland, S., Hudson, S. R., Hanson, S., Haapala, J., and Perovich, D. K.: Seasonality of spectral albedo and transmittance as observed in the Arctic Transpolar Drift in 2007, Journal of Geophysical Research-Oceans, 115, Artn C11011
Doi 10.1029/2009jc006074, 2010a.

Nicolaus, M., Hudson, S. R., Gerland, S., and Munderloh, K.: A modern concept for autonomous and continuous measurements of spectral albedo and transmittance of sea ice, Cold Regions Science and Technology, 62, 14-28, 2010b.

Nicolaus, M., Katlein, C., Maslanik, J., and Hendricks, S.: Changes in Arctic sea ice result in increasing light transmittance and absorption, Geophysical Research Letters, 39, submitted, Artn L24501
Doi 10.1029/2012gl053738, 2012.

Nicolaus, M., Arndt, S., Katlein, C., Maslanik, J., and Hendricks, S.: Correction to "Changes in Arctic sea ice result in increasing light transmittance and absorption", Geophysical Research Letters, 40, 2699-2700, 10.1002/grl.50523, 2013.

Perovich, D. K.: The Optical Properties of Sea Ice, U.S. Cold Reg. Res. and Eng. Lab. Monogr., Hannover, 25 pp, 1996.

Perovich, D. K., Roesler, C. S., and Pegau, W. S.: Variability in Arctic sea ice optical properties, Journal of Geophysical Research-Oceans, 103, 1193-1208, 10.1029/97jc01614, 1998.

Perovich, D. K., Grenfell, T. C., Light, B., and Hobbs, P. V.: Seasonal evolution of the albedo of multiyear Arctic sea ice, Journal of Geophysical Research-Oceans, 107, Artn 8044
Doi 10.1029/2000jc000438, 2002.

Perovich, D. K.: On the aggregate-scale partitioning of solar radiation in Arctic sea ice during the Surface Heat Budget of the Arctic Ocean (SHEBA) field experiment, Journal of Geophysical Research-Oceans, 110, Artn C03002
Doi 10.1029/2004jc002512, 2005.

Perovich, D. K., Light, B., Eicken, H., Jones, K. F., Runciman, K., and Nghiem, S. V.: Increasing solar heating of the Arctic Ocean and adjacent seas, 1979‐2005: Attribution and role in the ice ‐ albedo feedback, Geophysical Research Letters, 34, 2007a.

Perovich, D. K., Nghiem, S. V., Markus, T., and Schweiger, A.: Seasonal evolution and interannual variability of the local solar energy absorbed by the Arctic sea ice-ocean system, Journal of Geophysical Research-Oceans, 112, Artn C03005
Doi 10.1029/2006jc003558, 2007b.

Perovich, D. K., and Richter-Menge, J. A.: Loss of Sea Ice in the Arctic*, Annual Review of Marine Science, 1, 417-441, 2009.

Perovich, D. K., Jones, K. F., Light, B., Eicken, H., Markus, T., Stroeve, J., and Lindsay, R.: Solar partitioning in a changing Arctic sea-ice cover, Annals of Glaciology, 52, 192-196, 2011a.

Perovich, D. K., Richter-Menge, J. A., Jones, K. F., Light, B., Elder, B. C., Polashenski, C., Laroche, D., Markus, T., and Lindsay, R.: Arctic sea-ice melt in 2008 and the role of solar heating, Annals of Glaciology, 52, 355-359, 2011b.

Perovich, D. K., and Polashenski, C.: Albedo evolution of seasonal Arctic sea ice, Geophysical Research Letters, 39, Artn L08501
Doi 10.1029/2012gl051432, 2012.

Popova, E. E., Yool, A., Coward, A. C., Dupont, F., Deal, C., Elliott, S., Hunke, E., Jin, M. B., Steele, M., and Zhang, J. L.: What controls primary production in the Arctic Ocean? Results from an intercomparison of five general circulation models with biogeochemistry, Journal of Geophysical Research-Oceans, 117, Artn C00d12
Doi 10.1029/2011jc007112, 2012.

Ricker, R., Hendricks, S., Helm, V., Skourup, H., and Davidson, M.: Sensitivity of CryoSat-2 Arctic sea-ice freeboard and thickness on radar-waveform interpretation, The Cryosphere, 8, 1607-1622, 2014.

Rösel, A., and Kaleschke, L.: Exceptional melt pond occurrence in the years 2007 and 2011 on the Arctic sea ice revealed from MODIS satellite data, Journal of Geophysical Research-Oceans, 117, 10.1029/2011jc007869, 2012.

Rösel, A., Kaleschke, L., and Birnbaum, G.: Melt ponds on Arctic sea ice determined from MODIS satellite data using an artificial neural network, Cryosphere, 6, 431-446, 10.5194/tc-6-431-2012, 2012.

Stroeve, J. C., Markus, T., Boisvert, L., Miller, J., and Barrett, A.: Changes in Arctic melt season and implications for sea ice loss, Geophysical Research Letters, 41, 1216-1225, Doi 10.1002/2013gl058951, 2014.

Wang, C., Granskog, M. A., Gerland, S., Hudson, S. R., Perovich, D. K., Nicolaus, M., Ivan Karlsen, T., Fossan, K., and Bratrein, M.: Autonomous observations of solar energy partitioning in first ‐ year sea ice in the Arctic Basin, Journal of Geophysical Research: Oceans, 119, 2066-2080, 2014.

Wassmann, P., and Reigstad, M.: Future Arctic Ocean seasonal ice zones and implications for pelagic-benthic coupling, 2011.

**Figure 1**: Classification of sea ice (a) types and (b) surface properties as used in this study. The timing of each phase results from the status of the sea ice. Depending on the season, different sea ice types co-exist. Abbreviations: FYI: first year ice, MYI: multi year ice, EMO: early melt onset, MO: melt onset, EFO: early freeze onset, FO: freeze onset.

**Figure 2**: (a) Total transmittance of sea ice during each phase, as derived from previous field campaigns and observations (Fig. 1). In this figure, melt pond concentrations of 26 % are assumed for first year ice (FYI) and 29 % are assumed for multi year ice (MYI). (b) Transmittance of bare ice during each phase (see Figure 1). Transmittances of single ice classes are given in Table 1. The transmittance of open water is assumed as 0.93 for the entire seasonal cycle. Abbreviations: see Figure 1.

**Figure 3**: Monthly mean of total solar heat input ($Q_T(x,y)$) under Arctic sea ice (ice covered areas only) from April to September 2011. The months October to March resulted in fluxes < $0.4\ 10^{19}$ J, and are therefore not shown here.

**Figure 4**: Annual total solar heat input ($Q_T(x,y)$) through Arctic sea ice. (a) Average and (b) trend from 1979 to 2011. The trend is corrected for the trend in sea ice concentration. Purple shaded areas were not covered with sea ice during the maximum extent in all years.

**Figure 5**: Arctic-wide total solar heat flux under sea ice ($Q_T$) (black) and monthly Arctic-wide solar heat input for May to August (colored) and its trend from 1979 to 2011. The data are corrected for the trend in sea ice concentration. Areas that were not ice covered at any time in 2011 or in the certain month in 2011 are excluded from the analyses.

**Figure 6**: (a) Transmitted total solar heat input and (b) total transmittance during the drift of Tara in 2007 (*Nicolaus et al.,* 2010b). Compared are in situ measurements (green) with the presented method (red) and the presented method, but using the observed dates for phase transitions. Between 16 July and 14 August (dotted lines) a comparison is not reasonable since the sensor was strongly influenced by biological processes during Tara.

**Figure 7**: Changes in annual total solar heat input ($Q_T(x,y)$) through sea ice in 2011, resulting from a sensitivity study assuming an extended melt season. (a) 14 days earlier early melt onset and melt onset and (b) 14 days later early freeze onset and freeze onset than in the reference method, based on *Markus et al.* (2007).

**Table 1:** Data sources of the different parameters used in this study.

| Parameter | Time period | Source |
|---|---|---|
| Sea ice concentration | 1979 – 2007<br>2008 – 2011 | OSI SAF, reprocessed data<br>OSI SAF, operated data<br>(*Andersen et al.*, 2007) |
| Sea ice age | 1979 – 2011 | (*Maslanik et al.*, 2007;2011) |
| Downward surface solar radiation | 1979 – 2011 | ECMWF (*Dee et al.*, 2011) |
| Melt and freeze onset | 1979 – 2005<br>2006 – 2010<br>2011 | SSMR<br>AMSR-E<br>SSM/IS (*Markus et al.*, 2011) |
| Melt pond fraction | 1979 – 1999<br>2000 – 2011 | Constant fraction as in 2011<br>ICDC (*Rösel et al.*, 2012) |

**Table 2:** Transmittances of different sea ice and surface types. Abbreviations: FYI: first year ice, MYI: multi year ice, Phase I: winter, MO: melt onset, Phase IV: summer, FO: freeze onset, Threshold: transition from open ocean to sea ice and vice versa.

| | **Phase I (winter)** | **At MO** | **Phase IV (summer)** | **At FO** | **Threshold** |
|---|---|---|---|---|---|
| FYI, pond covered sea ice | 0.002 | 0.04 | 0.087 | 0.04 | 0.4 |
| MYI, pond covered sea ice | 0.002 | 0.02 | 0.05 | 0.02 | 0.4 |
| FYI, bare ice/snow | 0.001 | 0.017 | 0.04 | 0.017 | 0.17 |
| FYI, melt ponds | 0.22 | | | | |
| MYI, bare ice/snow | 0.0 | 0.004 | 0.01 | 0.004 | 0.07 |
| MYI, melt ponds | 0.15 | | | | |
| Open ocean | 0.93 | | | | |

**Table 3**: Annual Arctic-wide solar heat input under sea ice ($Q_T$). Results from the reference data set in 2011 and the sensitivity studies for 2011 (Case 1). All numbers in $10^{19}$ J and relative changes in %. Setups of the sensitivity studies are described in the text. The months October to March resulted in fluxes < 0.4 $10^{19}$ J.

| | Reference system | Changing EMO and MO | | | Changing EFO and FO | | |
|---|---|---|---|---|---|---|---|
| | | - 4 days | - 7 days | - 14 days | - 4 days | - 7 days | - 14 days |
| Apr | 1.00 | 1.17 (+17%) | 1.19 (+19%) | 1.45 (+45%) | 1.00 (0%) | 1.00 (0%) | 1.00 (0%) |
| May | 5.53 | 6.64 (+20%) | 7.35 (+33%) | 10.5 (+90%) | 5.53 (0%) | 5.53 (0%) | 5.53 (0%) |

| | | | | | | | |
|---|---|---|---|---|---|---|---|
| June | 20.9 | 22.8 (+9%) | 24.0 (+15%) | 27.1 (+30%) | 20.9 (0%) | 20.9 (0%) | 20.9 (0%) |
| Jul | 18.4 | 18.7 (+2%) | 19.1 (+4%) | 19.7 (+7%) | 18.4 (0%) | 18.4 (0%) | 18.4 (0%) |
| Aug | 6.33 | 6.34 (0%) | 6.42 (+1%) | 6.48 (+2%) | 6.46 (+2%) | 6.51 (+3%) | 6.68 (+5%) |
| Sep | 0.69 | 0.69 (0%) | 0.69 (0%) | 0.69 (0%) | 0.74 (+7%) | 0.81 (17%) | 0.97 (+41%) |
| All Year | 53.3 | 57.0 (+7%) | 59.2 (+11%) | 66.3 (+24%) | 53.4 (0%) | 53.6 (+0%) | 53.9 (+1%) |

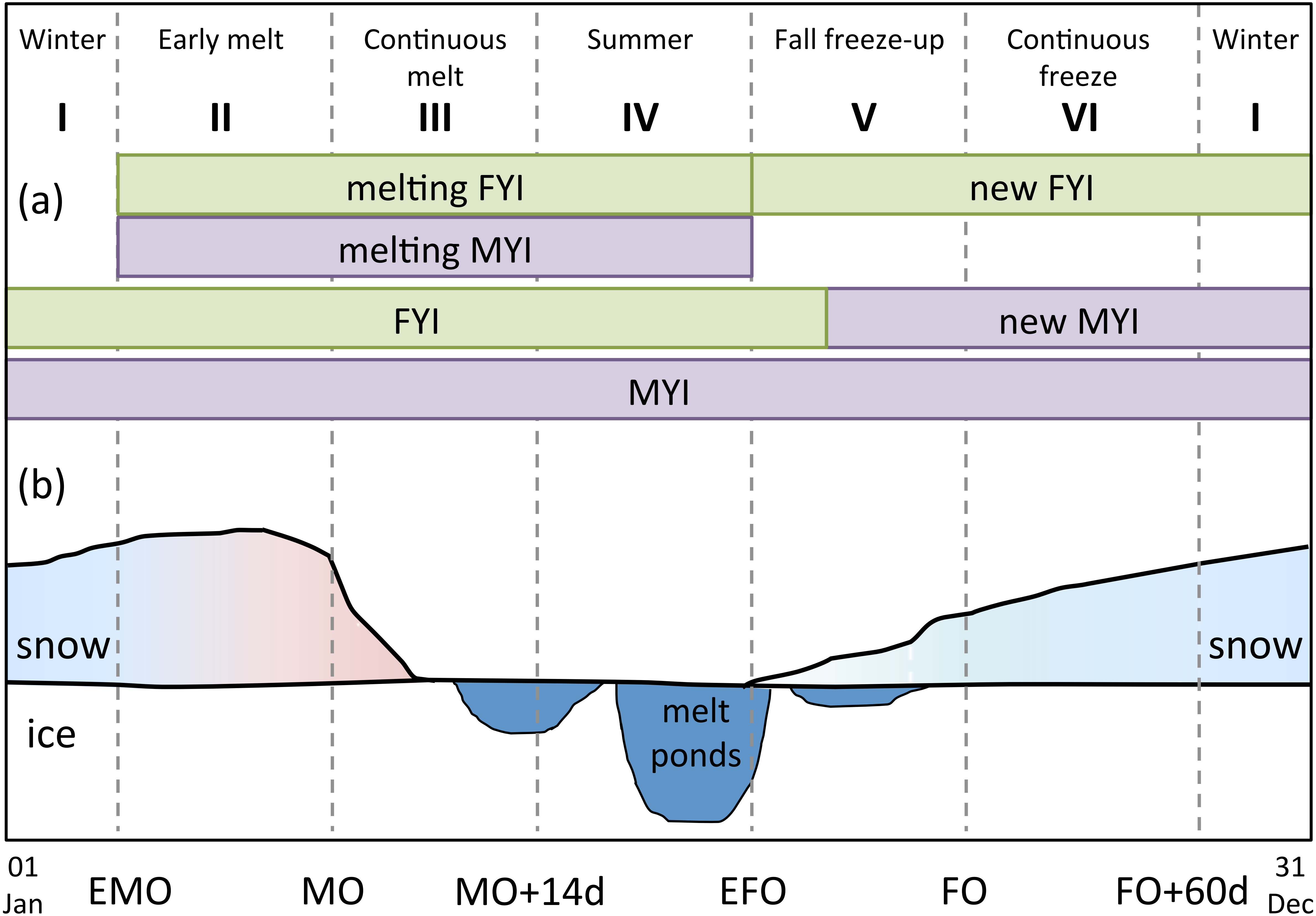

Winter
Early melt
Continuous melt
Summer
Fall freeze-up
Continuous freeze
Winter
I
II
III
IV
V
VI
I
(a)
melting FYI
new FYI
melting MYI
FYI
new MYI
MYI
(b)
snow
snow
ice
melt ponds
01 Jan
EMO
MO
MO+14d
EFO
FO
FO+60d
31 Dec

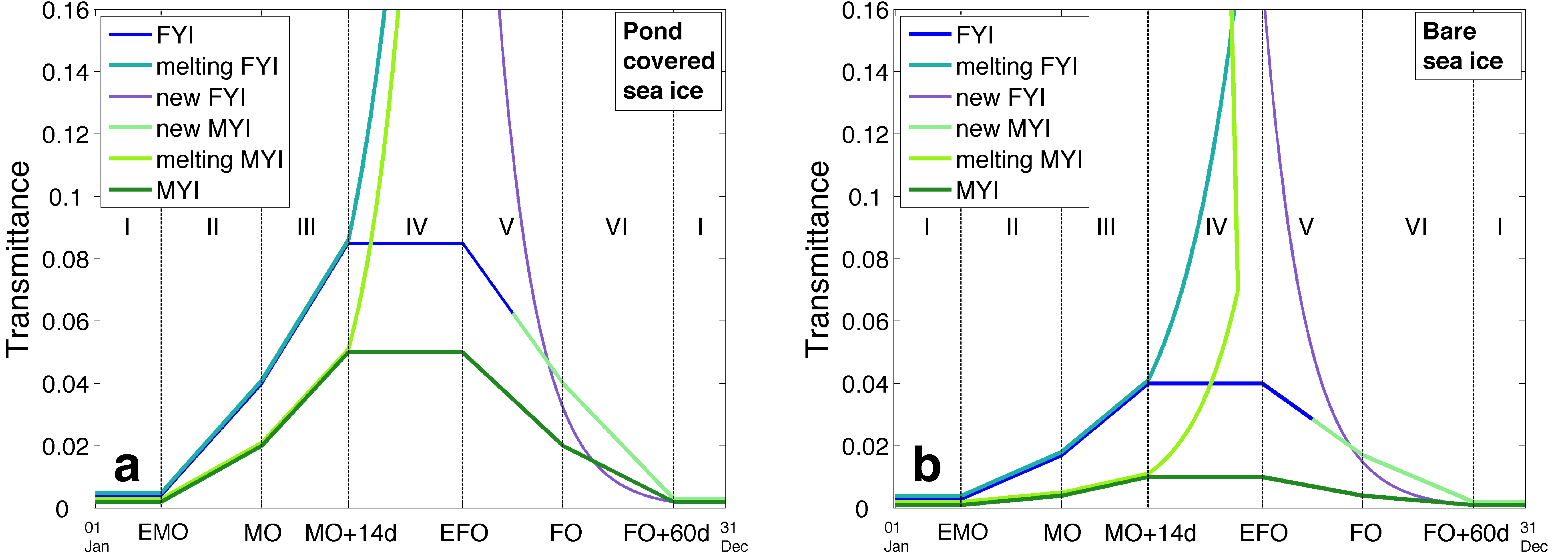

Transmittance
0.16
0.14
0.12
0.1
0.08
0.06
0.04
0.02
0
FYI
melting FYI
new FYI
new MYI
melting MYI
MYI
Pond covered sea ice
Bare sea ice
I
II
III
IV
V
VI
I
a
b
01 Jan
EMO
MO
MO+14d
EFO
FO
FO+60d
31 Dec

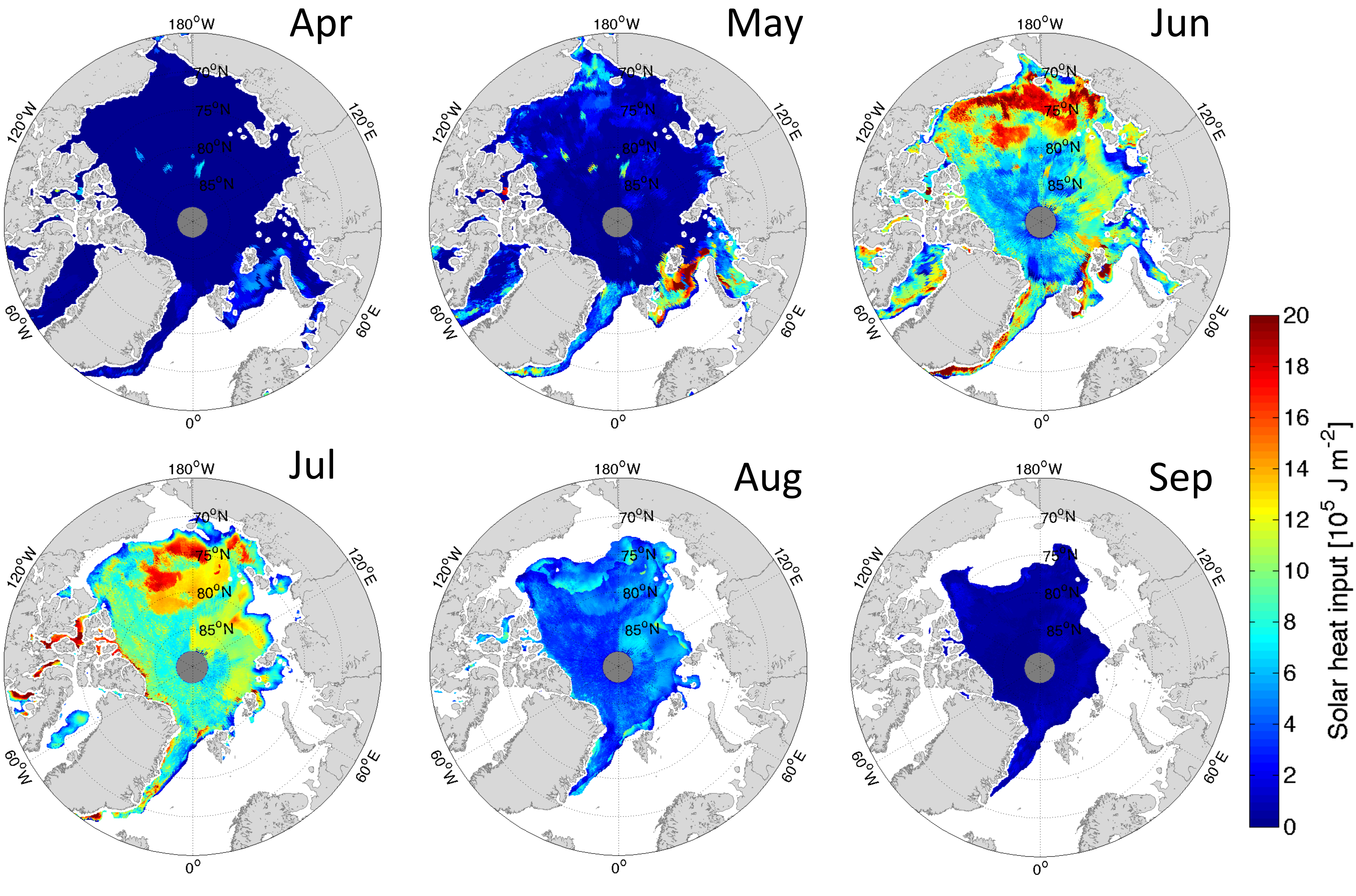
Apr
May
Jun
Jul
Aug
Sep
180°W
120°W
120°E
60°W
60°E
0°
70°N
75°N
80°N
85°N
Solar heat input [$10^5$ J $m^{-2}$]
0
2
4
6
8
10
12
14
16
18
20

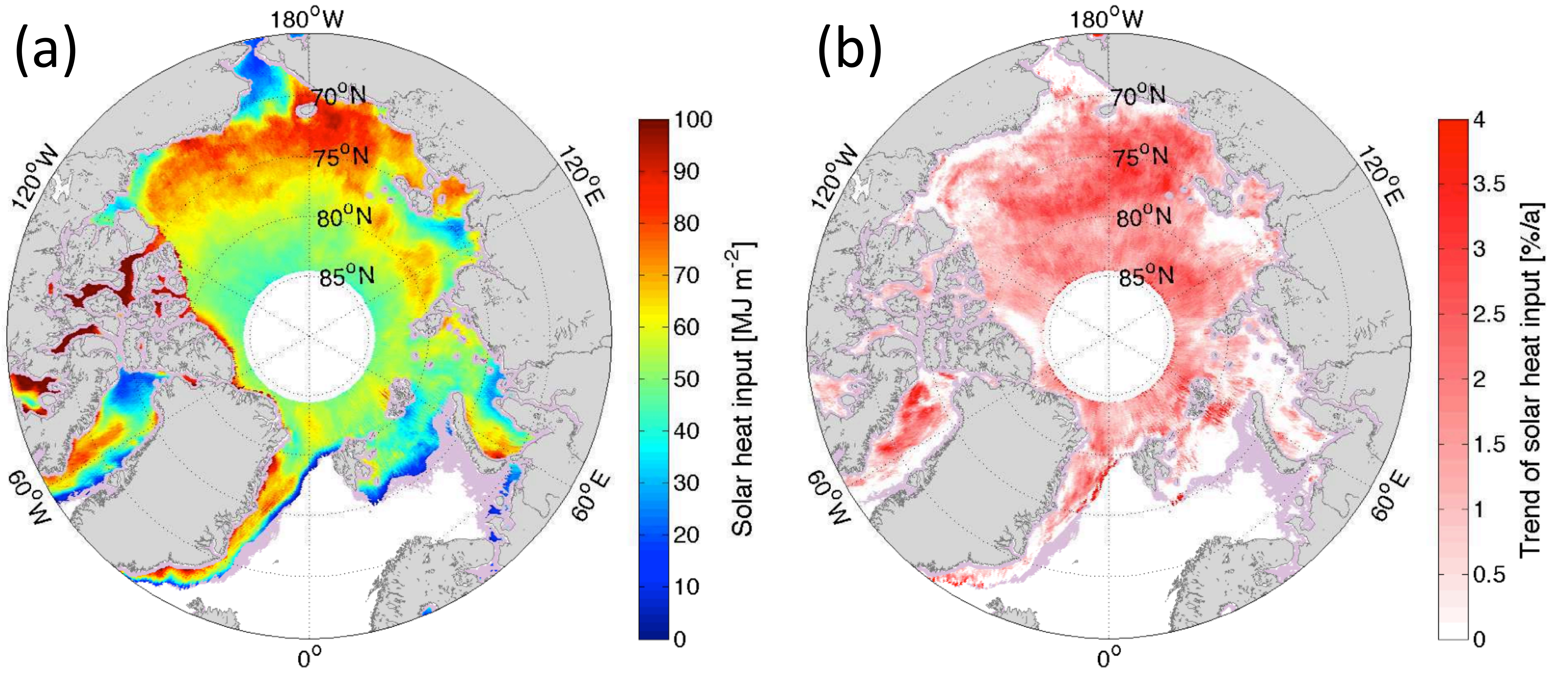
(a)
180°W
70°N
75°N
80°N
85°N
120°W
120°E
60°W
60°E
0°
Solar heat input [MJ m^-2]
100
90
80
70
60
50
40
30
20
10
0
(b)
180°W
70°N
75°N
80°N
85°N
120°W
120°E
60°W
60°E
0°
Trend of solar heat input [%/a]
4
3.5
3
2.5
2
1.5
1
0.5
0

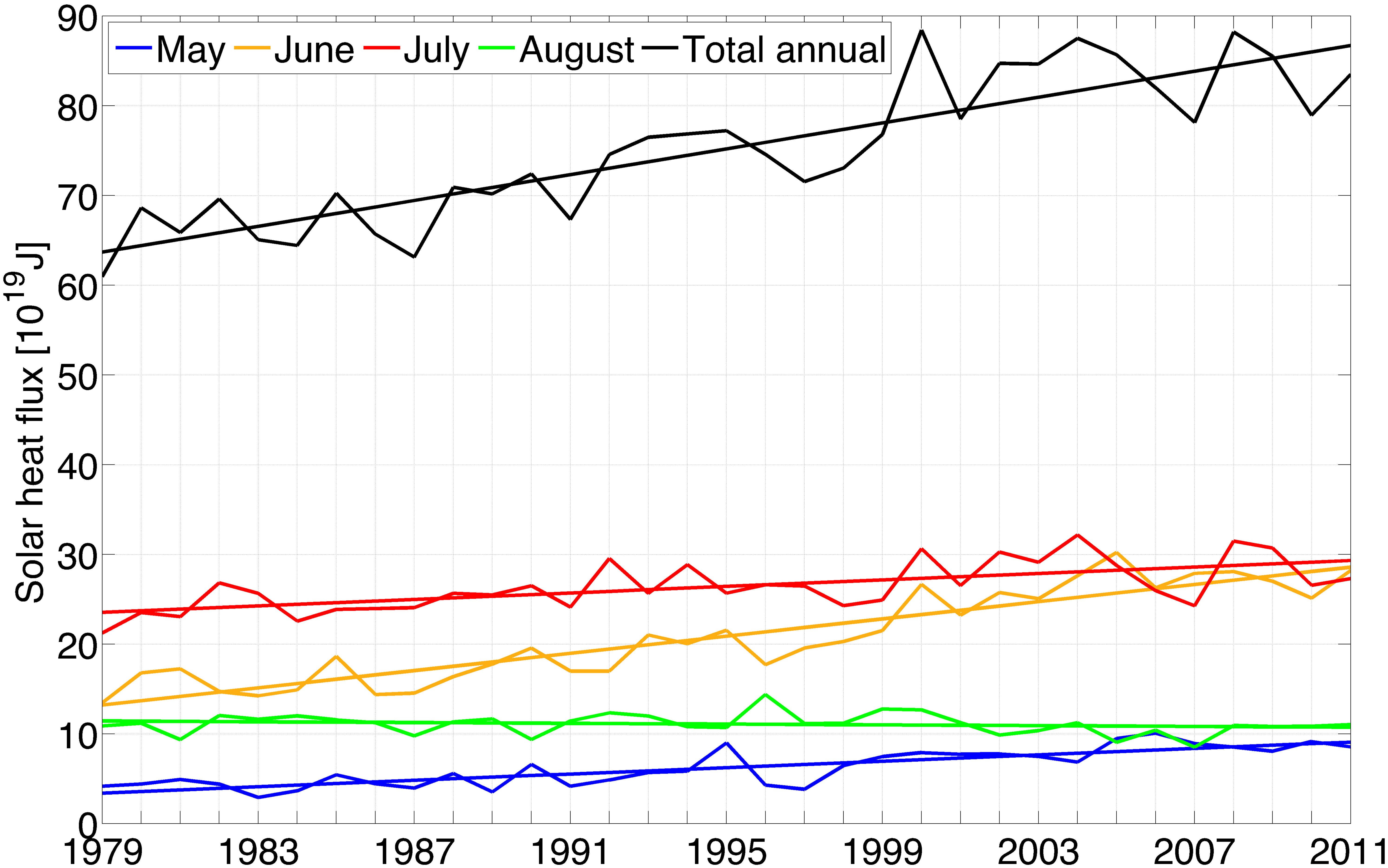

May
June
July
August
Total annual
Solar heat flux [$10^{19}$ J]
0
10
20
30
40
50
60
70
80
90
1979
1983
1987
1991
1995
1999
2003
2007
2011

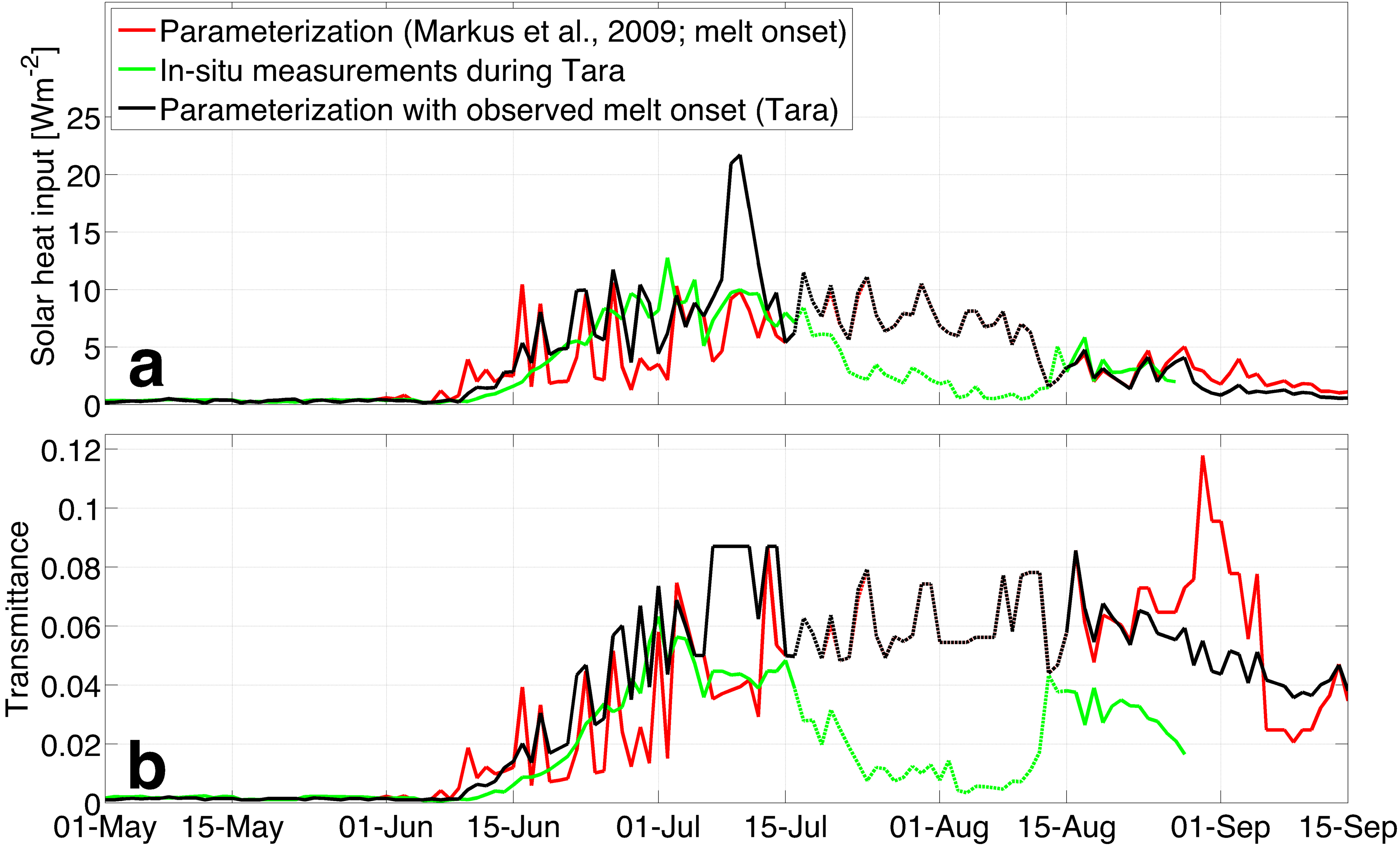

Parameterization (Markus et al., 2009; melt onset)
In-situ measurements during Tara
Parameterization with observed melt onset (Tara)
Solar heat input [Wm-2]
a
b
Transmittance
01-May
15-May
01-Jun
15-Jun
01-Jul
15-Jul
01-Aug
15-Aug
01-Sep
15-Sep

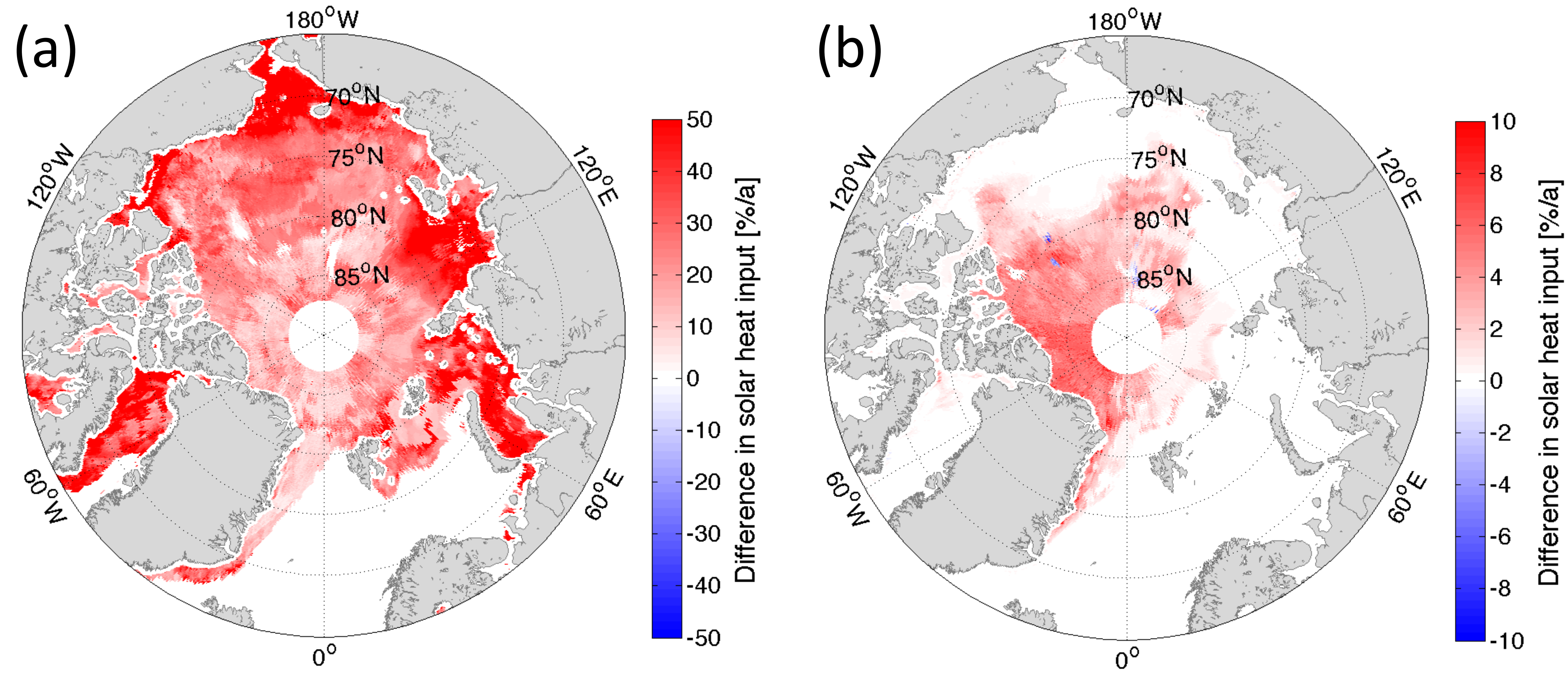

(a)
180°W
70°N
75°N
80°N
85°N
120°W
120°E
60°W
60°E
0°
50
40
30
20
10
0
-10
-20
-30
-40
-50
Difference in solar heat input [%/a]
(b)
180°W
70°N
75°N
80°N
85°N
120°W
120°E
60°W
60°E
0°
10
8
6
4
2
0
-2
-4
-6
-8
-10
Difference in solar heat input [%/a]